Phase diagram of $CeFeAs_{1-x}P_xO$ obtained from electrical resistivity, magnetization, and specific heat measurements

Yongkang Luo,[1] Yuke Li,[1] Shuai Jiang,[1] Jianhui Dai,[2] Guanghan Cao,[1] and Zhu-an Xu[1,*]
[1]*State Key Laboratory of Silicon Materials and Department of Physics, Zhejiang University, Hangzhou 310027, China*
[2]*Department of Physics, Zhejiang University, Hangzhou 310027, China*
(Received 20 October 2009; revised manuscript received 29 March 2010; published 19 April 2010)

We performed a systematic study on the properties of $CeFeAs_{1-x}P_xO$ ($0 \leq x \leq 1$) by electrical resistivity, magnetization, and specific heat measurements. The *c*-axis lattice constant decreases significantly with increasing P content, suggesting a remarkable chemical pressure. The Fe 3*d* electrons show the enhanced metallic behavior upon P doping and undergo a magnetic quantum phase transition around $x \approx 0.4$. Meanwhile, the Ce 4*f* electrons develop a ferromagnetic order near the same doping level. The ferromagnetic order is vanishingly small around $x=0.9$. The data suggest a heavy-fermionlike behavior as $x \geq 0.95$. No superconductivity is observed down to 2 K. Our results show the ferromagnetic ordered state as an intermediate phase intruding between the antiferromagnetic bad metal and the nonmagnetic heavy-fermion metal and support the cerium-containing iron pnictides as a unique layered Kondo lattice system.

DOI: 10.1103/PhysRevB.81.134422 PACS number(s): 75.20.Hr, 71.20.Eh, 74.70.Dd, 75.40.−s

I. INTRODUCTION

The homologous quaternary iron pnictides, *R* Fe *X*O, (*R*: rare earths, *X*: As or P) show a diversity of physical properties although they have the same ZrCuSiAs-type crystal structure with a unique Fe *X* layer sandwiched by the *R*O layer.[1] Typically, LaFeAsO is an antiferromagnetic (AFM) metal below 140 K and is a superconductor (SC) with maximal $T_c=26$ K upon F doping.[2] T_c can be surprisingly increased up to 41 K when La is replaced by Ce (Ref. 3) or even higher if replaced by other rare earths.[4–6] Meanwhile, the parent compounds (denoted as Ln-1111) of these SC's, such as CeFeAsO, are still Fe 3*d* itinerant AFM's similar to LaFeAsO. However, a noticeable *f*-electron AFM ordering of Ce^{3+} is also observed at a much lower temperature (~ 4 K).[3] On the other hand, the stoichiometric LaFePO is a low-T_c SC without any trace of the AFM ordering.[7,8] By contrast, CeFePO is a heavy-fermion (HF) metal with Kondo temperature $T_K \sim 10$ K.[9]

These discoveries put the rare-earth iron pnictides on the boundary between the high-T_c superconductors[10] and the heavy-fermion metals,[11] and open an avenue for searching the complicated interplay of various *d*- and *f*-electron correlations. Within the iron-pnictogen layer, the *d* electrons are expected to be more itinerant in the phosphides than in the arsenides,[12,13] with the former being recently identified as a moderately correlated metal.[14] In contrast to the cuprates, the interlayer distance between the transition metals and the rare earths in the iron pnictides is critically significant so that the coupling between them may play an important role even in the parent compounds of the high-T_c Fe-based SC's.[15] Recent neutron-scattering and muon-spin-relaxation experiments indeed provide evidence for a sizable interlayer coupling in CeFeAsO.[16,17] So far it is still unclear whether this coupling is due to some kind of polarization effect raised by the ordered moment of Fe^{2+} ions[17] or more microscopically the effective hybridization between the 3*d* and 4*f* orbitals bridged by the pnictogens.[15] A first-principle local-density approximation (LDA) plus dynamical mean-field theory (DMFT) study[18] suggested that applying a physical pressure will enhance the *d*-*f* hybridization, leading to the Kondo screening of the Ce moments. However a sufficiently high pressure is required in order to observe this effect. It turns out that $CeFeAs_{1-x}P_xO$, i.e., P doping at As sites in CeFeAsO, may provide, among others, a unique layered Kondo lattice system to probe the intriguing 3*d*-4*f* electron interplay under ambient pressure.[15] Chemical-pressure-induced superconductivity has been observed in P-doped LaFeAsO.[19]

We report a systematic study on the doping evolution of the physical properties of $CeFeAs_{1-x}P_xO$ using electrical resistivity $\rho(T)$, magnetic susceptibility $\chi(T)$, isothermal magnetization $M(H)$, and specific heat $C(T)$ measurements. A series of 21 different P-doped polycrystalline samples were synthesized. Our results reveal a rich phase diagram consisting of an AFM quantum critical point (QCP) of the Fe 3*d* electrons and a possible ferromagnetic (FM) QCP of the Ce 4*f* electrons. An intermediate FM phase emerges in between the AFM bad metal and the nonmagnetic HF metal. Because P doping does not introduce extra electrons but shortens the *c* axis significantly, these findings provide a rare example of chemical-pressure-induced HF metals with strong FM fluctuations.

II. EXPERIMENTAL

We synthesized a series of $CeFeAs_{1-x}P_xO$ ($0 \leq x \leq 1$) polycrystalline samples by solid-state reaction, during which, Ce, Fe, As, P, and CeO_2 of high purity ($\geq 99.95\%$) were used as starting materials. First, CeAs (or CeP) was presynthesized by reacting Ce disks and As (or P) powders at 1323 K for 72 h. FeAs (or FeP) was prepared by reacting Fe and As (or P) powders at 1173 K (or 1023 K) for 20 h. Second, powders of CeAs, CeP, CeO_2, FeAs, and FeP were weighed according to the stoichiometric ratio, thoroughly ground, and pressed into a pellet under a pressure of 600 MPa in an argon-filled glove box. The pellet was sealed into an evacu-

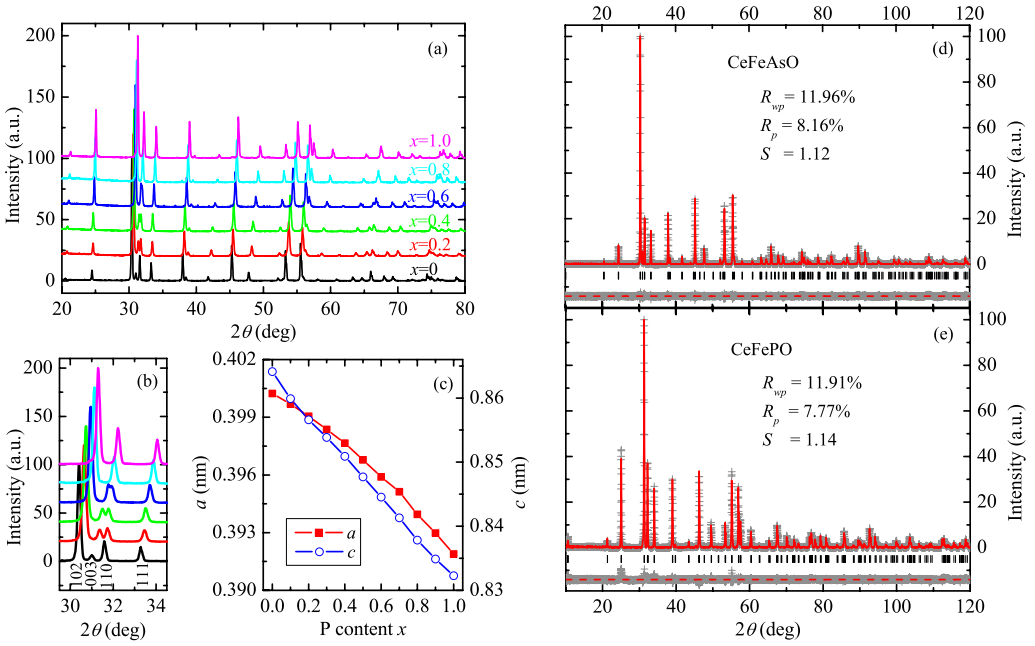

FIG. 1. (Color online) (a) XRD patterns of $x=0$, 0.2, 0.4, 0.6, 0.8, and 1.0 measured at room temperature. (b) Expanded XRD patterns showing the peak shift with the P doping. (c) Lattice parameters as functions of P-doping level. [(d) and (e)] Rietveld refinement profiles of CeFeAsO and CeFePO. The refined atomic coordinates (x,y,z) are: Ce (0.25, 0.25, 0.1411), O (0.75, 0.25, 0), Fe (0.75, 0.25, 0.5), As (0.25, 0.25, 0.6547) for CeFeAsO; and Ce (0.25, 0.25, 0.1508), O (0.75, 0.25, 0), Fe (0.75, 0.25, 0.5), P (0.25, 0.25, 0.6384) for CeFePO.

ated quartz tube, which was then slowly heated to 1448 K and kept at that temperature for 50 h.

Powder x-ray diffraction (XRD) was performed at room temperature using a D/Max-rA diffractometer with Cu $K\alpha$ radiation and a graphite monochromator. Lattice parameters were refined by a least-squares fit using at least 30 XRD peaks and the structural refinements were performed using the program RIETAN 2000. The dc magnetization measurement was carried out in a Quantum Design magnetic property measurement system (MPMS-5). Physical property measurement system (PPMS-9) was used to take the resistivity measurement, as well as specific heat.

III. RESULTS AND DISCUSSION

The room-temperature powder XRD patterns of $CeFeAs_{1-x}P_xO$ are shown in Fig. 1. All the XRD peaks can be well indexed based on the tetragonal ZrCuSiAs-type structure with the space group $P4/nmm$ (No. 129), and no obvious impurity phases can be detected, suggesting high quality of the samples. As shown in Figs. 1(a) and 1(b), the XRD peaks shift toward right hand, especially for the high angle reflections. The (003) peaks shift much faster than the (110) peaks so that they merge into one peak in the high-doping case, indicating that the c axis shrinks more severely than the a axis. This observation is consistent with the lattice-parameter calculation results shown in Fig. 1(c). Figures 1(d) and 1(e) present the Rietveld refinement profiles for the two end members CeFeAsO and CeFePO, which give details of the crystal structure. The remarkable differences in structure lie in the positions of Ce and As/P. For CeFePO, the thickness of FeP layers is much smaller, meanwhile, Ce atomic layers are much closer to the FeP layers. This structural feature supports the strong coupling between Fe $3d$ and Ce $4f$ electrons.

The temperature-dependent resistivity is shown in Fig. 2, where four prominent features can be identified. (i) The overall suppression of the room-temperature resistivity with increasing doping. The resistivity at $T=300$ K decreases gradually from 300 $\mu\Omega$ m for $x=0$ to 12 $\mu\Omega$ m for $x=1$, indicating that P doping enhances the metallic behavior significantly. (ii) The resistivity anomaly, mostly pronounced for $x=0$. This anomaly was ascribed to the structure distortion and the accompanied Fe-AFM transition.[20,21] Upon doping, the anomaly is suppressed monotonically and soon becomes an unremarkable kink at lower temperatures. No clear kink can be identified for $x>0.3$. The suppression of this anomaly with P doping is consistent with the suppression of AFM order of Fe ions, which is confirmed by a recent neutron study.[22] We mark arrows in Fig. 2(a) to show the Fe-AFM transition (T_{N1}, data from Ref. 22). (iii) The resistivity upturn at low temperatures for $x\leq 0.4$. The upturn behavior is suppressed by doping or magnetic field, see the inset of Fig. 2(b). (iv) The metallic behavior in the entire measured temperature range for $x>0.4$. In particular, the resistivity drops rapidly at low temperatures for larger x. Such a drop in resistivity has already been observed in the HF metal CeFePO in the previous report.[9] However, no SC is observed down to $T=2$ K for the entire P-doping range.

It should be noted that the value of resistivity itself may not reflect the polycrystalline sample's quality. Actually the most likely impurity phases in the Ln-1111 pnictides could be FeAs or Fe_2As, and Ln_2O_3. Both FeAs and Fe_2As are highly metallic, more metallic than CeFeAsO itself at low temperatures. The metallic impurity phase such as FeAs

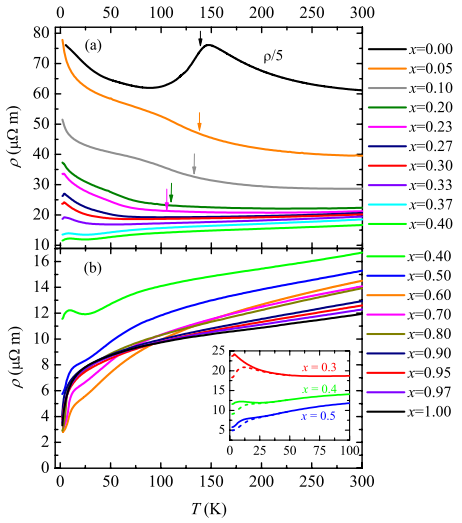

FIG. 2. (Color online) Temperature dependence of resistivity in $CeFeAs_{1-x}P_xO$. (a) For $0 \leq x \leq 0.4$. Arrows denotes the temperature of Fe-AFM order, T_{N1}, which were taken from Ref. 22. (b) For $0.4 \leq x \leq 1$. The inset shows the resistivity of $x=0.3$, 0.4, and 0.5, under zero field (solid lines) and $\mu_0 H$ of 5 T (dashed lines).

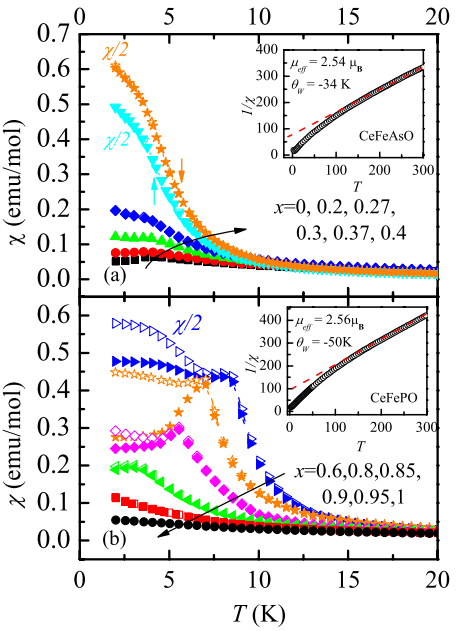

FIG. 3. (Color online) Temperature dependence of dc magnetic susceptibility under ZFC (solid symbols) and FC (open symbols) protocols for $CeFeAs_{1-x}P_xO$ samples under a magnetic field of 1000 Oe. Arrows are guide to eyes to indicate the FM transition temperature T_C which is defined from the extrapolation of $1/\chi$-T plot. The insets show the Curie-Weiss behavior of susceptibility above 150 K for CeFeAsO and CeFePO, respectively.

could distribute most likely in the grain boundaries and thus result in a lower resistivity if the main phase is a bad metal. The intrinsic resistivity behavior of Ln-1111 parent pnictides below the Fe-AFM order is still ambiguous. For example, the resistivity of single crystal of LaFeAsO shows an upturn at low temperatures,[23] meanwhile the resistivity of both polycrystalline and single-crystalline CeFeAsO samples shows clear metallic behavior.[3,24] However, our more than 20 $CeFeAs_{1-x}P_xO$ samples with different P content were prepared under same conditions and the XRD patterns show that they all are of same high purity, the systematic decrease in resistivity indeed suggests the increasing metallicity with increasing P content.

The temperature dependence of dc magnetic susceptibility is shown in Fig. 3. In the high-temperature range, $\chi(T)$ increases with decreasing temperature down to 150 K following a Curie-Weiss law for all $0 \leq x \leq 1$. The derived effective moment μ_{eff} is $2.54\mu_B$ for $x=0$, and $2.56\mu_B$ for $x=1$ [insets of Fig. 3], very close to that of a free Ce^{3+} ion, $2.54\mu_B$. By lowering temperatures, a clear peak was observed at 4.16 K for $x=0$, related to the formation of the Ce^{3+} AFM order. With increasing x, $\chi(T)$ increases and the peak becomes round (or shoulderlike); meanwhile the corresponding AFM ordering temperature does not change too much. For $x \gtrsim 0.4$, an obvious divergence between zero-field cooling (ZFC) and field cooling (FC) is seen at lower temperatures [see Fig. 3(b)], manifesting the FM ordered ground state of the Ce $4f$ electrons. The suppression of AFM and development of FM are consistent with the enhanced metallic transport behavior in the course of P doping. The FM ordered state persists until $x \sim 0.9$ where the divergency of $\chi(T)$ vanishes.

The evolution of Ce^{3+} magnetism can be further demonstrated by isothermal field-dependent magnetization measurements, which are shown in Fig. 4. The temperatures are fixed at 2 K and 10 K, respectively. For $x=0$ and $T=2$ K, a kink in the magnetization curve is clearly seen, indicating a possible spin flop in the AFM state of Ce^{3+}. When x increases the kink becomes weaker. As $x \geq 0.4$, $M(H)$ starts to increase rapidly for small fields and tends to saturate at higher fields, i.e., it exhibits a nonlinear field dependence, see Fig. 4(d) for $x=0.4$. For $0.5 \lesssim x < 0.9$, a clear hysteresis loop can be observed and the saturated M value reaches the maximum around $x=0.6$ [see Fig. 4(e)]. Therefore, the long-range FM order exists in a wide doping range in between $x \sim 0.4$ and $x \sim 0.9$. The largest saturated magnetic moment is about $0.95\mu_B$, close to $1\mu_B$ expected for a Ce^{3+} doublet ground state.[9,16] For $0.9 \lesssim x < 0.95$ the hysteresis loop is hardly observable down to the lowest measured temperature while the saturation tendency persists. This may be due to strong FM fluctuations at the quantum critical point associated with the $4f$ electrons. On the other hand, both the susceptibility and magnetization show a nonmagnetic HF-like phase for $x \geq 0.95$ [see Figs. 3(b), 4(g), and 4(h)], consistent with the resistivity measurement.

The metallic HF-like behavior can be further manifested by the specific heat measurement as shown in Fig. 5. For $x=0.95$, 0.97, and 1, the specific heat coefficient $\gamma(T) = C(T)/T$ shows $-\log T$ behavior at low temperatures down to 2 K, see the inset of Fig. 5. We define a characteristic temperature T_γ (below which HF-like behavior appears) as the intersection of two extrapolate lines of the specific heat data. For the $x=1$ sample, $T_\gamma \sim 8.6$ K. The saturated γ should be about 700–800 mJ/mol K^2 or larger, in agreement with the result of Ref. 9, where γ increases in proportion to $-\log T$ before it gets saturated below 1 K. As a comparison, $\gamma(T)$ shows a λ peak maximized around 4.2 K and

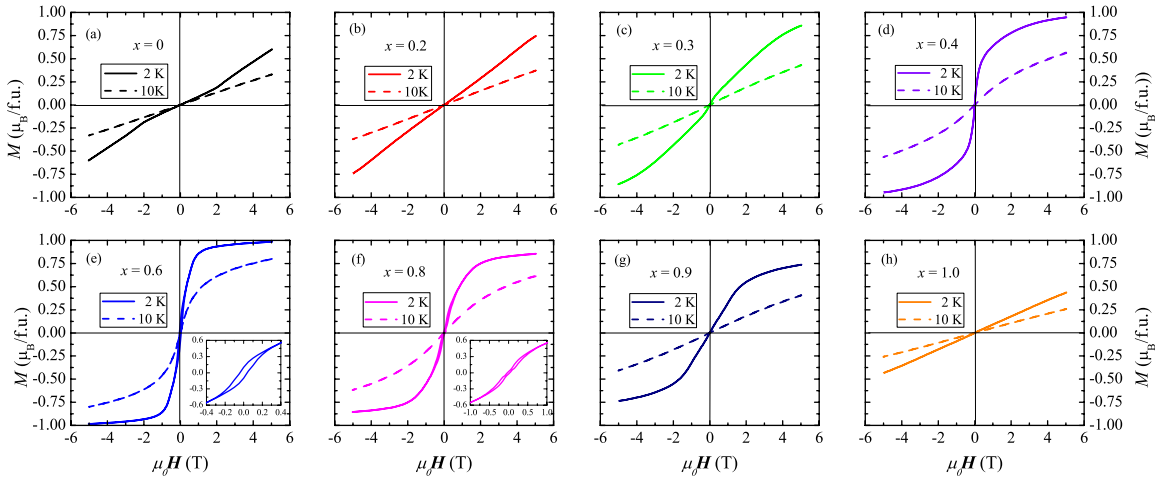

FIG. 4. (Color online) Isothermal magnetization of $CeFeAs_{1-x}P_xO$. (a) $x=0$. (b) $x=0.2$. (c) $x=0.3$. (d) $x=0.4$. (e) $x=0.6$. (f) $x=0.8$. (g) $x=0.9$. (h) $x=1.0$. For clarity, only the data of 2 K (solid lines) and 10 K (dashed lines) are shown. The insets of (e) and (f) display the magnetic hysteresis loop at 2 K.

6.8 K in the AFM and FM ordered phases, for $x=0$ and 0.8, respectively, in agreement with the magnetization measurement. A sudden increase in the saturated γ close to $x\sim0.9$ can be inferred by the values of $\gamma(T=2\ \mathrm{K})$, accompanied by a decrease in the saturated magnetization under $\mu_0 H=5$ T. This implies the enhancement of the Kondo screening near the FM instability. It should be noted that a very tiny kink was observed around 6 K on the C/T-T curve of $x=0.95$. We ascribe this additional peak to the contribution from some impurities with lower P content. Roughly estimated from the intensity of the kink, the amount of the impurity phase should be less than 2%.

We summarize the experimental results by suggesting an electronic phase diagram shown in Fig. 6. At low temperatures, both the Fe $3d$ and Ce $4f$ electrons show the long-range AFM ordering for $x\lesssim0.37$. The d electrons are Pauli paramagnetic (PM) for $x\gtrsim0.4$ while the f electrons are FM ordered until $x\sim0.9$. For $x\geq0.95$, the f moments are completely quenched and the whole system becomes a nonmagnetic HF-like metal. The HF-like region is roughly depicted by T_γ. Therefore, in addition to the first magnetic QCP (denoted by x_{c_1}) associated with the AFM-PM transitions of the d electrons, there could be another QCP associated with the FM-HF transition of f electrons around x of 0.92 (denoted by x_{c_2}). x_{c_1} has been known to be 0.4 by the study of neutron scattering.[22] A turning point (denoted by x_{c_3}) associated with the AFM-FM transition of the f electrons at $x_{c_3}\sim0.37$ is quite close to x_{c_1}. Meanwhile the strong FM fluctuations show up in the vicinity of x_{c_2}.

It should be noticed that the transition temperatures of the Fe-AFM ordering and the structure distortion can be ap-

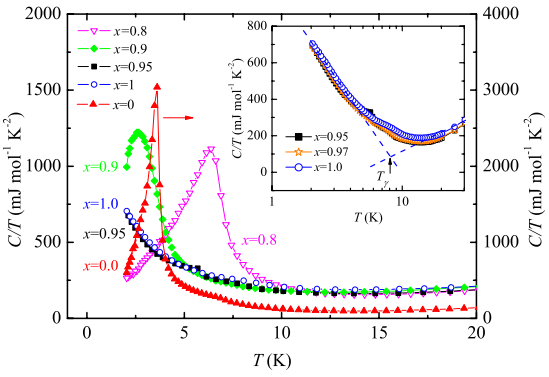

FIG. 5. (Color online) Specific heat measurements of $CeFeAs_{1-x}P_xO$. A λ peak can been observed around $T=4.2$ K and 6.8 K for $x=0$ and 0.8, respectively, corresponding to the AFM and FM transitions. Inset: for $x=0.95$, 0.97, and 1, the specific heat coefficient $\gamma(T)=C(T)/T$ shows $-\log T$ behavior at low temperatures down to 2 K and tends to saturate to $\gamma(0)$ when $T\rightarrow0$. The $\gamma(0)$ value was extrapolated to be about 700–800 $\mathrm{mJ/K^2}$ mol or larger for $x=1.0$.

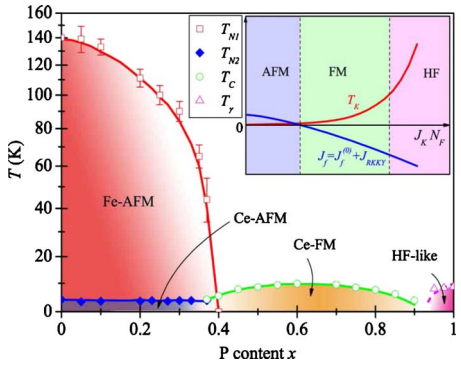

FIG. 6. (Color online) Electronic phase diagram of $CeFeAs_{1-x}P_xO$ $(0\leq x\leq1)$. The shaded region (in red) in the left side shows the antiferromagnetic ordering of Fe $3d$ moments [denoted by Fe-AFM below T_{N1} (Ref. 22)]. In the lower temperature portion of this region, simultaneously, Ce $4f$ moments order antiferromagnetically (marked with Ce-AFM) below T_{N2}. The small pink area at the lower right corner displays the nonmagnetic state with HF behavior. In the lower middle regime (in green), the $4f$ moments are ferromagnetically ordered (labeled by Ce-FM) below T_C. Inset: the schematic competition between J_f and T_K accounting for the AFM-FM-HF evolution of the f electrons.

proximately determined from the resistivity anomaly as shown in Fig. 2 and neutron studies.[22] They are undistinguishable in resistivity when $x>0.2$. The neutron study[22] revealed that both of them are suppressed at $x_{c_1}\sim 0.4$, confirming an early theoretical prediction for the existence of a unique magnetic QCP driven by P doping.[25] Moreover, the *d*-electron QCP seems to be very close to the turning point (x_{c_3}) of the *f* electrons. This fact may indicate that the *d*-electron magnetic transition is of weak first order accompanied by a reconstruction of the electronic states across x_{c_1}. It is not certain if the coincidence implies the AFM ordering in Ce subsystem being supported by the AFM order in the Fe plane because the ordering patterns of the two subsystems are different and the *f*-electron AFM order can coexist with the *d*-electron SC order in the F-doping case.[3,20] Besides this puzzling feature, other implications of our experimental results should be addressed as follows.

First, as the suppression of the *a* axis is only a fraction of that of the *c* axis upon P doping, the electronic states within the Ce-O layer should not change significantly. This is also supported by the nonmagnetic LDA calculation from which the different Fermi surfaces of CeFeAsO and CeFePO can be mainly ascribed to the pnictogen height.[18,26] Therefore the HF behavior in the end compound, CeFePO, is originated unambiguously from the interlayer coupling between the Fe 3*d* and Ce 4*f* electrons. Second, the *f*-electron AFM-FM transition could be explained by assuming the existence of a bare *d*-*f* Kondo coupling (J_K) in the ordered phases, as it can mediate the indirect Ruderman-Kittel-Kasuya-Yosida (RKKY) interaction (J_{RKKY}) between the Ce 4*f* local moments. Intuitively, the exchange interaction between the local *f* spins, J_f, is given by $J_f=J_f^{(0)}+J_{\mathrm{RKKY}}$, with $J_f^{(0)}$ being the exchange interaction in the absence of J_K and $|J_{\mathrm{RKKY}}|\sim J_K^2 N_F$, with N_F being the density of states (DOS) at Fermi level (of mainly *d*-electron characteristic). J_{RKKY} is negative if N_F is small, as it should be since the parent compound CeFeAsO is a bad metal.[12,13] Upon P doping, both J_K and N_F should increase, leading to a sign change in J_f. Third, the negative J_f is also the driving force for the strong FM fluctuations in the vicinity of the critical point x_{c_2}, where the Kondo scale T_K (which increases exponentially with $J_K N_F$) starts to dominate over the magnetic ordering energy scale, $T_f\approx|J_f|$.

It is well established that the RKKY interaction between the local moments is mediated by the Kondo coupling between the itinerant charge carries and local moments.[27,28] The Kondo coupling can lead to both the Kondo effect and the RKKY interaction with the latter being responsible to the magnetic ordering of the local moments. The crucial point is that the dependences on the Kondo coupling (together with the DOS of the charge carries) of the Kondo energy scale (describing the Kondo effect) and of the RKKY interaction (characterizing the ordering temperature of the local moments) are different, as described by the intuitive formulas in the inset of Fig. 6. Based on the similar intuitive formulas, Doniach first suggested that a quantum phase transition from magnetic ordering phase to the paramagnetic HF phase could exist in a Kondo lattice.[27] Here, we suggest that the AFM-FM-HF evolution of the *f* electrons in $CeFeAs_{1-x}P_xO$ is due to the competition between T_K and J_f (instead of J_{RKKY} in the conventional Kondo lattice[11]), see the inset of Fig. 6. Notice that $J_f^{(0)}$ is positive and relatively small in the absence of J_{RKKY}. Thus in the AFM phase T_K is mainly suppressed by the AFM ordering gap of the *d* electrons.[15] This picture provides a natural explanation for the strong FM fluctuations in a class of homologous HF compounds including CeFePO (Ref. 9) and CeRuPO.[29,30] Therefore the observed *f*-electron phase diagram of $CeFeAs_{1-x}P_xO$ system is consistent with the Doniach picture.[27] In addition, it also predicts a possible weak Kondo phase in a narrow doping region enclosing the turning point x_{c_3} (at very low temperatures). As x_{c_3} is very close to x_{c_1}, it may account for the observed suppression of the SC near the AFM QCP. The existence of this peculiar phase and its possible connection with the transport and magnetic properties still need to be clarified.

IV. CONCLUSION

In summary, our experimental study on $CeFeAs_{1-x}P_xO$ ($0\leq x\leq 1$) reveals a rich phase diagram which consists of an AFM quantum phase transition of the Fe 3*d* electrons and an AFM-FM-HF evolution of the Ce 4*f* electrons. The AFM QCP of the *d* electrons is very close to the turning point of the AFM-FM transition of the *f* electrons while the *d*-*f* hybridized HF state is separated by an *f*-electron FM instability. In contrast to the F-doping case where the high-T_c SC is induced, no SC is observed down to 2 K in the present case, signaling the unique role of P doping in suppressing the *d*-electron correlation.[13,25] These results highlight the importance of the interlayer Kondo physics[15,31] and the interplay of the *d*- and *f*-electron correlations in the rare-earth iron pnictides.

ACKNOWLEDGMENTS

We thank Xi Dai and Huiqiu Yuan for helpful discussions. This work is supported by the National Science Foundation of China, the PCSIRT (Grant No. IRT-0754), and the National Basic Research Program of China (Grants No. 2007CB925001 and No. 2009CB929104).

*zhuan@zju.edu.cn

[1] R. Pottgen, and D. Johrendt, Z. Naturforsch. **63b**, 1135 (2008).
[2] Y. Kamihara, T. Watanabe, M. Hirano, and H. Hosono, J. Am. Chem. Soc. **130**, 3296 (2008).
[3] G. F. Chen, Z. Li, D. Wu, G. Li, W. Z. Hu, J. Dong, P. Zheng, J. L. Luo, and N. L. Wang, Phys. Rev. Lett. **100**, 247002 (2008).
[4] X. H. Chen, T. Wu, G. Wu, R. H. Liu, H. Chen, and D. F. Fang, Nature (London) **453**, 761 (2008).

[5] Z. A. Ren, W. Lu, J. Yang, W. Yi, X. L. Shen, C. Zheng, G. C. Che, X. L. Dong, L. L. Sun, F. Zhou, and Z. X. Zhao, Chin. Phys. Lett. **25**, 2385 (2008).
[6] C. Wang, L. Li, S. Chi, Z. Zhu, Z. Ren, Y. Li, Y. Wang, X. Lin, Y. Luo, X. Xu, G. Cao, and Z. Xu, EPL **83**, 67006 (2008).
[7] Y. Kamihara, H. Hiramatsu, M. Hirano, R. Kawamura, H. Yanagi, T. Kamiya, and H. Hosono, J. Am. Chem. Soc. **128**, 10012 (2006).
[8] D. H. Lu, M. Yi, S. K. Mo, A. S. Erickson, J. Analytis, J. H. Chu, D. J. Singh, Z. Hussain, T. H. Geballe, I. R. Fisher, and Z. X. Shen, Nature (London) **455**, 81 (2008).
[9] E. M. Brüning, C. Krellner, M. Baenitz, A. Jesche, F. Steglich, and C. Geibel, Phys. Rev. Lett. **101**, 117206 (2008).
[10] P. A. Lee, Rev. Mod. Phys. **78**, 17 (2006).
[11] P. Coleman, in *Handbook of Magnetism and Advanced Magnetic Materials*, edited by H. Kronmuller and S. Parkin (Wiley, New York, 2007), Vol. 1, pp. 95–148; see also arXiv:cond-mat/0612006 (unpublished).
[12] Q. Si and E. Abrahams, Phys. Rev. Lett. **101**, 076401 (2008).
[13] Q. Si, E. Abrahams, J. Dai, and J. X. Zhu, New J. Phys. **11**, 045001 (2009).
[14] M. M. Qazilbash, J. J. Hamlin, R. E. Baumbach, L. Zhang, D. J. Singh, M. B. Maple, and D. N. Basov, Nat. Phys. **5**, 647 (2009).
[15] J. Dai, J. X. Zhu, and Q. Si, Phys. Rev. B **80**, 020505(R) (2009).
[16] S. Chi, D. T. Adroja, T. Guidi, R. Bewley, S. Li, J. Zhao, J. W. Lynn, C. M. Brown, Y. Qiu, G. F. Chen, J. L. Lou, N. L. Wang, and P. Dai, Phys. Rev. Lett. **101**, 217002 (2008).
[17] H. Maeter, H. Luetkens, Y. G. Pashkevich, A. Kwadrin, R. Khasanov, A. Amato, A. A. Gusev, K. V. Lamonova, D. A. Chervinskii, R. Klingeler, C. Hess, G. Behr, B. Büchner, and H. H. Klauss, Phys. Rev. B **80**, 094524 (2009).
[18] L. Pourovskii, V. Vildosola, S. Biermann, and A. Georges, EPL **84**, 37006 (2008).
[19] C. Wang, S. Jiang, Q. Tao, Z. Ren, Y. Li, L. Li, C. Feng, J. Dai, G. Cao, and Z. Xu, EPL **86**, 47002 (2009).
[20] J. Zhao, Q. Huang, C. de la Cruz, S. Li, J. W. Lynn, Y. Chen, M. A. Green, G. F. Chen, G. Li, Z. Li, J. L. Luo, N. L. Wang, and P. Dai, Nature Mater. **7**, 953 (2008).
[21] C. Hess, A. Kondrat, A. Narduzzo, J. E. Hamann-Borrero, R. Klingeler, J. Werner, G. Behr, and B. Büchner, EPL **87**, 17005 (2009).
[22] C. de la Cruz, W. Z. Hu, S. Li, Q. Huang, J. W. Lynn, M. A. Green, G. F. Chen, N. L. Wang, H. A. Mook, Q. Si, and P. Dai, Phys. Rev. Lett. **104**, 017204 (2010).
[23] J.-Q. Yan, S. Nandi, J. L. Zarestky, W. Tian, A. Kreyssig, B. Jensen, A. Kracher, K. W. Dennis, R. J. McQueeney, A. I. Goldman, R. W. McCallum, and T. A. Lograsso, Appl. Phys. Lett. **95**, 222504 (2009).
[24] A. Jesche, C. Krellner, M. de Souza, M. Lang, and C. Geibel, New J. Phys. **11**, 103050 (2009).
[25] J. Dai, Q. Si, J. X. Zhu, and E. Abrahams, Proc. Natl. Acad. Sci. U.S.A. **106**, 4118 (2009).
[26] V. Vildosola, L. Pourovskii, R. Arita, S. Biermann, and A. Georges, Phys. Rev. B **78**, 064518 (2008).
[27] S. Doniach, Physica B **91**, 231 (1977).
[28] A. C. Hewson, *The Kondo Problem to Heavy Fermions* (Cambridge University Press, Cambridge, England, 1993).
[29] C. Krellner, N. S. Kini, E. M. Brüning, K. Koch, H. Rosner, M. Nicklas, M. Baenitz, and C. Geibel, Phys. Rev. B **76**, 104418 (2007).
[30] C. Krellner, T. Förster, H. Jeevan, C. Geibel, and J. Sichelschmidt, Phys. Rev. Lett. **100**, 066401 (2008).
[31] A. H. Nevidomskyy and P. Coleman, Phys. Rev. Lett. **103**, 147205 (2009).